Project Title:

Computational Studies of Muon Locations, Electronic Structures and Electron Transport in High-Tc Superconductor, Organic, Organometallic and Biological Systems

Name:
[A,B]Shukri Sulaiman, [A,B]Mohamed Ismail Mohamed-Ibrahim, [B]Isao Watanabe, [A,B]Ainul Fauzeeha Rozlan, [A,B]Harison Rozak, [B,C]Fahmi Astuti, [B,C]Muhammad Darwis Umar, [B,C]Irwan Ramli, [B,C]Julia Angel, [B,D]Muhammad Redo Ramadhan, [B,E]Dita Puspita Sari, [B,E]Retno Asih, [B,F]Sungwon Yoon

Laboratory at RIKEN:
Advanced Meson Science Laboratory

[A]Universiti Sains Malaysia, Malaysia
[B]RIKEN, Nishina Center, Japan
[C]Hokkaido University, Japan
[D]Universitas Indonesia
[E]Osaka University, Japan
[F]The Catholic University of Korea

Description of the project

1. Background and purpose of the project, relationship of the project with other projects

The μSR spectroscopic technique is an excellent method to probe the electronic and magnetic properties of various condensed matter systems. It has been applied to study different classes of materials, for example, organic compounds, semiconductors, organometallic compounds and others as well. In order to complement the μSR experimental studies, DFT methods have been performed to computationally study the electronic structures of the target materials. The ultimate goal for our work is to understand the muon properties as a dilute magnetic probe and quantum electronic spin states surrounding muons in materials. In order to understand the experimental result by using muons, we need to investigate the most probable stopping sites for muon in the materials and the associated hyperfine interactions. μSR experimental technique is not able to confirm the position of muon owing to insufficient experimental information. The theoretical calculations on hyperfine interactions can be very valuable to obtain a general idea about the position of muon. By the comparison between experimental and computation results, we can reveal the quantum effects on the muon itself and the electronic spin states.

In this project, our research group has focused on the studies of muon in six different host materials. The materials are listed below along with their background study.

i. Organic magnets

We focus on two kinds of organic molecular systems. One is the series of $X[Pd(dmit)_2]_2$ and the other is the series of $(BEDT\text{-}TTF)_2X$. Both series have low-dimensional crystal structure and the basis is made of organic molecules. These are basically π electron conductors with either the anion or the cation parts being formed by dimers. An unpaired electron is normally localized in throughout the dimer and not localized around a particular atom which can affect the magnetic properties of the systems. As such, the long range ordering of the magnetic moments that make up the magnetic structure of the systems is not clear and remain to be investigated and confirmed. The determination of the magnetic structure is almost

not feasible experimentally due to issues with the samples such as the powder form and insufficient quantity. Thus, the magnetic structure has to be determined computationally by studying the exchange interactions. Characteristic interests of those target systems are as follows.

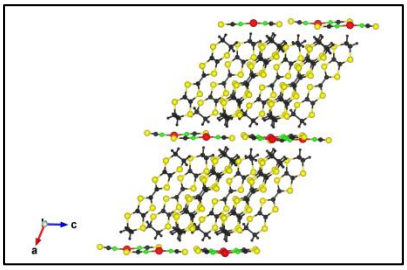

Figure 1: Example of (BEDT-TTF)$_2X$ crystal structure.

a) X[Pd(dmit)$_2$]$_2$ X=Et$_n$Me$_{4-n}$(P,Sb)

β'-X[Pd(dmit)$_2$]$_2$ radical salts where X is the cation, is one of a class of organic magnets that exhibit unusual electronic and magnetic properties. The cation X consists of $(CH_2CH_3)_n(CH_4)_{n-1}$(P, Sb). There are several experimental evidences indicating that these systems are Mott insulators with antiferromagnetic ordering. Manipulation of X, temperature, and pressure, however, will create variations in the electronic and magnetic phases of the compounds such as superconducting, Mott insulating, spin-liquid, valence bond solid and spin density wave ordering. This rich variety of phases could be attributed to the competition between spin frustration effects and electronic correlations that arise from the 2-dimensional triangular lattice arrangement of the spin ½ [Pd(dmit)$_2$]$_2$ dimer.

A full picture of the electronic structures of the pure and muonated β'-X[Pd(dmit)$_2$]$_2$ salts is the key to understanding the underlying physics behind the phenomenal characteristics of these organic magnets and also for the manipulation of the parameters to synthesize new compounds with specific target properties.

b) EtMe$_3$Z[Pd(dmit)$_2$]$_2$ (Z=P, As)

We centered our study on the pressure-induced superconductor behavior, EtMe$_3$Z[Pd(dmit)$_2$]$_2$, (Z=P, As) system. The EtMe$_3$As[Pd(dmit)$_2$]$_2$ crystal system is β'-structure (monoclinic *C2/c*) and antiferromagnetic (AFM) ordering at T_N=23K. In contrast, the EtMe$_3$P[Pd(dmit)$_2$]$_2$ exhibits two different phases, major and minor phase. The monoclinic *P2$_1$/m* phase was obtained as the major phase, accompanied by triclinic- and β'-structure (monoclinic *C2/c*) as minor phases. The major phase, EtMe$_3$P[Pd(dmit)$_2$]$_2$ (*P2$_1$/m*) shows valence bond ordering at T_{VB}=25K. The β-EtMe$_3$Z[Pd(dmit)$_2$]$_2$, (Z=P, As) has a solid-crossing stacking structure which is the dimer unit stacking along the $a - b$ direction in the 1st layer and $a+b$ direction in the 2nd layer whereas the EtMe$_3$P[Pd(dmit)$_2$]$_2$ (*P2$_1$/m*) has parallel molecular stacking structure.

c) κ-(BEDT-TTF)$_2$Cu[N(CN)$_2$]Cl and
κ-d8-(BEDT-TTF)$_2$Cu[N(CN)$_2$]Br

The isostructural cation radical salts κ-(BEDT-TTF)$_2$Cu[N(CN)$_2$]Cl and κ-d8-(BEDT-TTF)$_2$Cu[N(CN)$_2$]Br are very interesting because their properties are tunable with respect to lattice parameters. These compounds are also organic magnet materials like the materials in 1 (a) and 1 (b). The difference is that for this systems the unpaired electron spin is localized throughout the cation which is forms by the dimers. We have already performed some μSR measurements on those systems and confirmed that long-range orderings appeared in those systems. The experimental results are about to be submitted to a journal.

ii. High temperature superconductor

In this category, we are interested in two systems, La_2CuO_4 and $YBa_2Cu_3O_6$. Both systems are strongly correlated Mott insulators. Since those systems

have been well investigated by μSR in the past, there is a lot of experimental data which are still required to be tested by DFT investigations. The important points of this theme are to investigate the quantum effects of the muon itself and the spin states in the systems. We are currently investigating the spatial distributions of the muon itself around a stopping position due to zero-point vibration motion as a light particle, and also investigating the spatial distribution of the electron spins due to strongly hybridized electron orbitals which is the fundamental behavior as these strongly correlated system. By taking into account the quantum effects, we expect the μSR experimental data and computational results are in good agreement. This finding can be applied to other strongly correlated systems to investigate their electronic states.

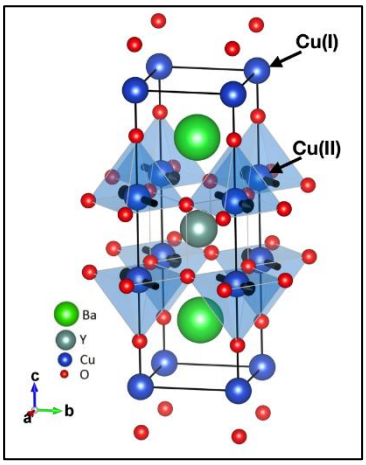

Figure 2: Crystal structure of $YBa_2Cu_3O_6$ with antiferromagnetic ordering at Cu (II) atoms.

iii. Synthesized simple and short strand DNA

Deoxyribonucleic acid (DNA) is a versatile molecule that stores genetic information and consists of two polynucleotide chains twisted around each other in the form of a double helix. DNA is formed using sequences of four nitrogenous bases. These four bases are guanine (G), adenine (A), cytosine (C) and thymine (T), and they can be divided into two groups. Guanine and adenine belong to the purine group. Cytosine and thymine on the other hand belong to the pyrimidine. Purines and pyrimidines are considered as aromatic compounds and are electron rich in nature. DNA bases provide an effective medium for electron transport because of overlap in the electron orbital of adjacent bases.

In this current computational project, which is the first stage of our studies on the electron transport in DNA, DFT cluster method was applied to study the electronic structures, muon trapping sites and hyperfine interactions in adenine, guanine, cytosine, and thymine to see the differences in nucleobases and nucleotides environments (Figure 3).

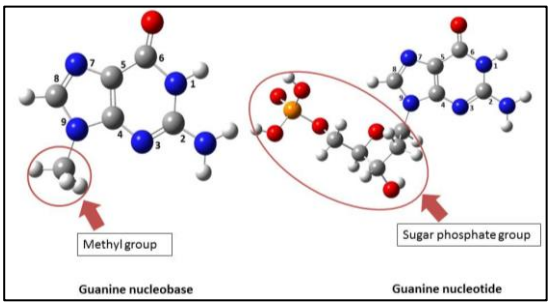

Figure 3: Guanine nucleobase and nucleotide structures.

These calculations were then extended by using a 12mer homogenous single strand DNA to see the changes in the electronic structure as we increase the number of bases and the effect of neighboring bases could be included. Four systems have been built which are short single strand DNA (ssDNA) molecules in the following forms (Figure 4):

1) 12mer single strand DNA oligomer with base sequence AAA… (adenine)
2) 12mer single strand DNA oligomer with base sequence TTT… (thymine)
3) 12mer single strand DNA oligomer with base sequence CCC… (cytosine)

4) 12mer single strand DNA oligomer with base sequence GGG… (guanine)

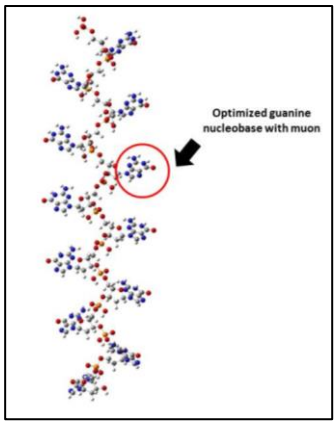

Figure 4: 12mer single strand guanine

The results obtained from these calculations will be further studied and discussed in relation with the experimental work. For the experiment, we have also prepared the four 12mer oligomer samples. The length of the synthetic DNA oligomers was designed to be 12 because it is the length of a complete one turn of the double helix DNA structure. The double helix structure will be studied after the completion of calculations for the single strand systems. Therefore, the changes in the electronic structures as the structure of the systems changes can be examined from the computational and experimental studies on the electron dynamics, muon positions and muon hyperfine interactions.

iv. Kitaev Honeycomb material

The honeycomb ruthenate, α-$RuCl_3$, was suggested as a proximate of the Kitaev honeycomb model, which could provide another approach to the quantum spin liquid on the honeycomb lattice. This system can be clarified as a spin-orbit entangled Mott insulator composed by the 4*d* transition metal ion, Ru^{3+}, with the Kramers doublet state and a strong spin-orbit coupling effect owing to the partially filled *d* level in the octahedral environment by surrounding anions, Cl^-. On the honeycomb network of transition metal ions, the Ising-like anisotropic exchange between the nearest neighboring transition metal ions emerges owing to the edge-shared octahedral. Since the anisotropic exchange is strongly dependent on the bonding path, and there are three different paths on the honeycomb network, the spin frustrated state would be revealed through the competition among anisotropic exchanges dependent on different bonding paths.

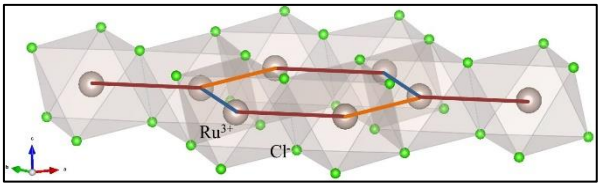

Figure 5: The honeycomb ruthenate with rhombohedral lattice

Previous μSR investigations exhibited the oscillating behavior, indicating the long-range magnetic ordering, and the maintenance of the fluctuations of electronic magnetic moments even in the ordered state. First-principles calculation using density functional theory was performed to understand the nature of the long-range ordered state in detail. By tuning the on-site Coulomb interaction, and Hund's coupling of the rhombohedral structured honeycomb ruthenate based on the DFT + U formalism, spin structures and exchange paths are expected to be extracted from the comparison between experimental results and theoretical estimations.

v. Gold nano-clusters

Metal nano-clusters such as Pt, Pd, Au, and Ag have become the focus of numerous studies due to their peculiar size-dependent electronic, optical, catalytic, and magnetic properties compared to their bulk counterparts. The nano-Au clusters have been intensively utilized in biological and medical fields. These include applications in diagnosis, therapy, drug or gene delivery, sensing, and imaging. An interesting and important fundamental research issue on the nano-Au cluster is whether Au becomes

magnetic as the dimension approaches nanometer scale. The first observation of significant magnetism in the nano-Au cluster that contains 144 Au atoms was reported in 2004. Ligand-stabilized nano-Au clusters are of high interest due to their fundamental physics as well as practical applications, such as high-density storage media and next generation devices like single electron transistors and nano-electronics.

vi. Alkalimetal Superoxides

Spin orbit coupling (SOC) in Mott insulators is an interesting physical phenomenon that has been intensively investigated in the last decade. It has been pointed out that SOC exists in 2*p* electron systems also, such as AO_2 (*A* = Na, K, Rb, and Cs) alkalimetal superoxides. Several theoretical investigations proposed that the half-metallic state was realized in those alkalimetal superoxides, while experimental results showed that AO_2 compounds are insulating. On the other hand, Kim *et al.* (2010) succeeded to describe the insulating electronic structure of KO_2 by using the generalized gradient approximation (GGA) with the on-site Coulomb interaction, U, between the oxygen 2*p* electrons (GGA+U). They included the SOC effect as the second variational procedure (GGA+U+SO). This study indicated the importance of the SOC effect and the crystal field from K^+ in order to describe the electronic state of the alkalimetal superoxides. Until recently, only KO_2 has been successfully studied. Thus, we are investigating the electronic state for RbO_2 and CsO_2 using the same method. The long-range ordering in both systems has been observed using μSR measurements. The goals of this project are to determine the magnetic spin structure of alkalimetal superoxides, their electronic states and to examine the effect of SOC and the differences among the alkalimetal. According to Riyadi *et al.* (2012) there is a structural phase transition in CsO_2. The crystal structure of CsO_2 is tetragonal at room temperature where the O_2 molecular bond axes are parallel to the z-axis while at low temperature, the O_2 molecular bond axes seem to tilt uniformly by 5^0 leading to a lower symmetry orthorhombic structure. As we expect a strong correlation between structural phase transition and magnetic exchange interaction in CsO_2, we have calculated the electronic properties in high and low symmetry structures.

2. Specific usage status of the system and calculation method

In our computational work, we utilized two software:

i) Gaussian 16
ii) Vienna Ab-initio Simulation Package (VASP) ver. 5.4

We used Gaussian16 to perform linear combination of atomic orbital molecular orbital (LCAO-MO) calculations, whereas VASP was utilized to perform calculations for band structure and spin structure. Most of our calculations were performed using VASP on the MPC resources since we need to use supercell with the muon to estimate the electronic state with quantum effects of the muon and electronic spins. We have utilized more than 85% of the initial MPC core time allocation on GW mainly for our supercell calculations using VASP to simulate dilute muon centers in the systems

We still need more core times to simulate the real environment in the muonated materials. In 2017, we have also applied for more core times in the new BW system. We were awarded with sufficient core times in the BW system and our plan on large-scale calculations, especially on the high-Tc systems, are now in progress. On the other hand, our calculations using Gaussian 16 require large memory. That is why we used ACSL to accomplish our Gaussian 16 calculations.

3. Result

In FY2017, the μSR experiments and computational studies, have been conducted on the materials described in Section 1 above. Large amount of μSR experimental data have been collected. These will be analyzed in conjunction with DFT calculations. The results of the computational work are discussed, separately by materials as listed below:

i) Organic magnets

We have performed first principle computational studies on the organic magnets in the antiferromagnetic state as well as examining the possible muon stopping sites. As for now, we have completed all calculations for three pure systems (without muon) and have started the calculations on the hyperfine interactions for the muonated systems.

At present, we are working on the dipole field calculations as well as the vibrational averaging for the hyperfine interactions. We are also in the preparation to submitting part of our work for publication.

Here, we present the results of our computational investigations on the (a) ß′-X[Pd(dmit)$_2$]$_2$, (b) EtMe3Z[Pd(dmit)$_2$]$_2$, (Z=P, As), and (c) (BEDT-TTF)$_2$X systems.

(a) *ß′*-X[Pd(dmit)$_2$]$_2$ X=EtnMe$_{4-n}$ (P, Sb)(n=0-4)

Figure 6 and 7 show the calculated relative energy and exchange coupling constants for three *ß′-X*[Pd(dmit)$_2$]$_2$ compounds with different AFM spin configurations. *X* consists of Me$_4$P, Et$_2$Me$_2$P and EtMe$_3$Sb. In the case of *X*= EtMe$_3$Sb, there are two possible orientations with 50% occupancy for each orientation. These differences are due the position of ethyl in the cation part that located is on a two-fold axis but it does not have a two-fold symmetry.

The possible AFM spin configurations consisting of (a)*AFM$_1$*, (b) *AFM$_2$*, and (c) *AFM$_3$* are shown in Figure 6. The results indicate that *AFM$_3$* spin configuration has the lowest energy as compared to other spin configurations. The relative energies are shown in the bar chart in Figure 7.

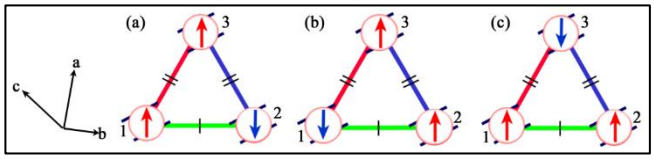

Figure 6: Schematic diagram of the 3-fragment cluster systems with three different AFM spin configurations labeled as (a) *AFM$_1$*, (b) *AFM$_2$*, and (c) *AFM$_3$*.

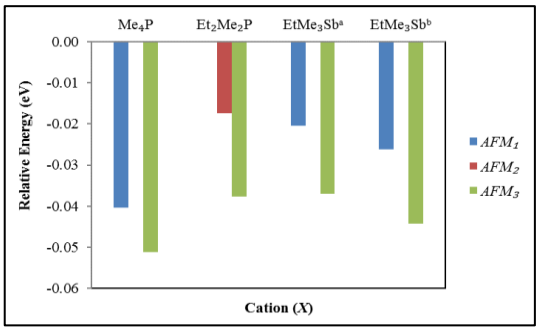

Figure 7: Relative energies for the 3-fragment cluster with different AFM spin configurations.

As shown in Figure 8, the exchange coupling constant between dimer 2 and dimer 3 which is denoted as J_{23} has the strongest interaction when the spins are stacked in the same column.

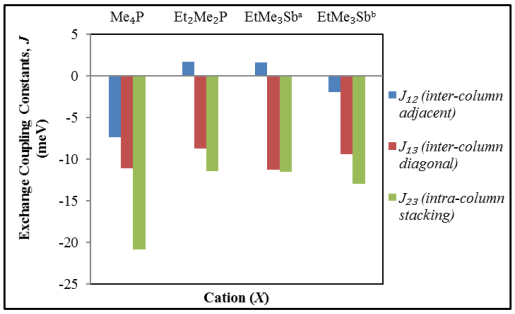

Figure 8: Exchange coupling constants between two magnetic centers.

a) $EtMe_3Z[Pd(dmit)_2]_2$ (Z=P, As)

In the one fragment cluster system, the calculated spin density shows that the spin is distributed throughout the dimer. The percentage of spin distribution for thiolate, thione, and thiol are ~59%, 15% and 2% respectively. The details on the percentage of spin distribution for $EtMe_3Z[Pd(dmit)_2]_2$, (Z=P, As) are shown in Figure 9 below.

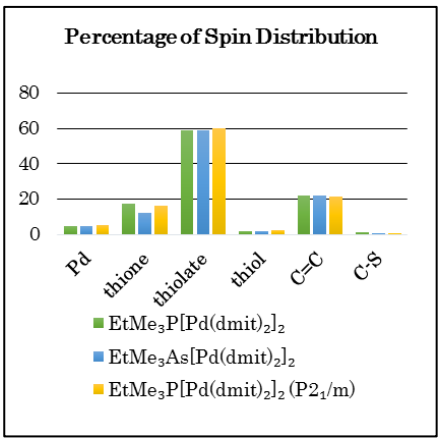

Figure 9: Percentage of Spin Distribution for $EtMe_3Z[Pd(dmit)_2]_2$, (Z=P, As).

We also considered possible AFM spin configurations as shown in Figure 6. The exchange coupling constant for the two fragments system is the highest for dimer 2 and 3 as shown in Figure 10. In addition, relative energy of the dimers in the intra-column stacking for the $EtMe_3P[Pd(dmit)_2]_2$ ($P2_1/m$) system is about seven times higher than the others.

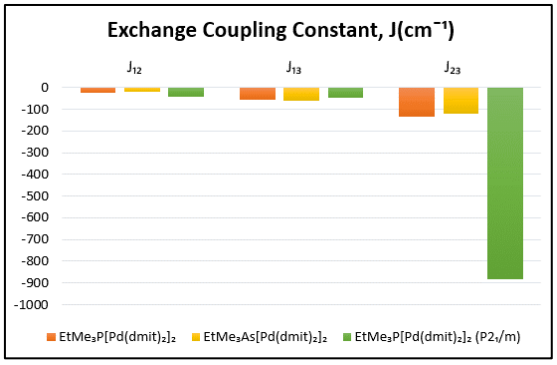

Figure 10: Exchange coupling constant for two fragments system.

In three fragments system, the calculation results show that the possible AFM configuration is AFM_3, has the lowest compared to other spin configuration. The relative energy of three fragments system is shown in Figure 11.

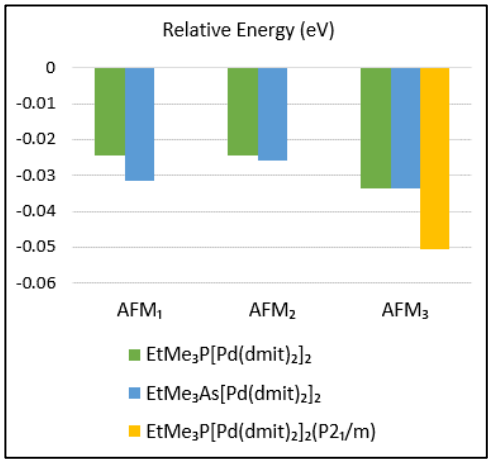

Figure 11: Relative energy for three fragments system with different AFM configuration.

b) κ-$(BEDT\text{-}TTF)_2Cu[N(CN)_2]Cl$ and κ-d8-$(BEDT\text{-}TTF)_2Cu[N(CN)_2]Br$

We have performed the calculations for this compound by using Gaussian16 available in ACSG resources. The results obtained from these calculations indicate that the spin densities are not localized on any particular atom but distributed throughout the cation. The distribution of the spin densities is clearly shown in Figure 12 below. For κ-d8-$(BEDT\text{-}TTF)_2Cu[N(CN)_2]Br$, the spin distributions are similar to the κ-$(BEDT\text{-}TTF)_2Cu[N(CN)_2]Cl$ compound.

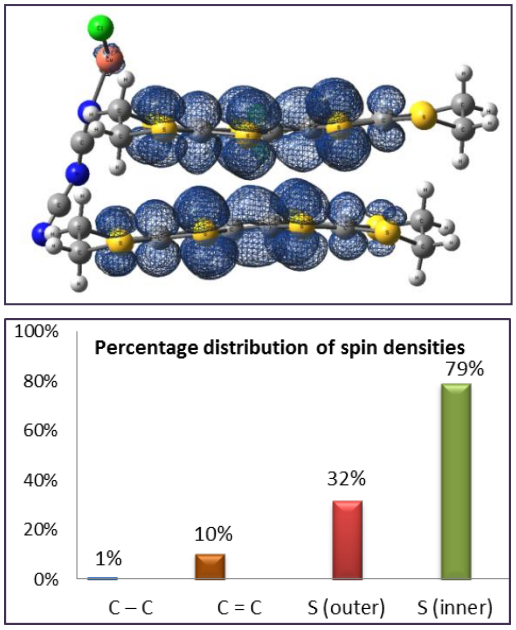

Figure 12: Distribution (top) and percentage (bottom) distribution of spin densities of κ-(BEDT-TTF)$_2$Cu[N(CN)$_2$]Cl.

From the determination of J values, we acquired the values for J1, J2 and J3 as 68.9 cm^{-1}, 3.6 cm^{-1} and -38.9 cm^{-1} respectively. From the three values, we found that only J3 shows AFM interaction due to the negative value of exchange coupling interaction obtained for J3 as shown in Figure 13. The value of J2 which is the interaction between dimer 2 (D2) and dimer 3 (D3) was found to be very small as compared to J1 and J3.

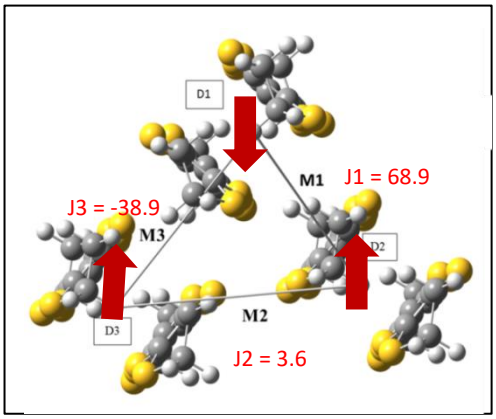

Figure 13: Values of the exchange coupling constants and the possible magnetic structure for κ-Cl is indicated by the red arrows.

ii) High temperature superconductor

a) La_2CuO_4

We have already carried out DFT calculations to check the band gap by using GGA exchange-correlation and applying the on-site Coulomb interaction with U = 8 eV. We have succeeded to confirm the opening of the gap around the Fermi level by using these conditions. We also observed the effect of local crystal deformation and the modification of spatial spin distributions caused by the injected muon. For the trial, we calculated a medium-class supercell which is 2 x 2 x 1 and contains four unit cells. From the electrostatic potential calculations, we found that there are three local minimum potential points where the muon prefer to stop initially just after its entry. We named these as M1, M2, and M3. These three points are shown in Figure 14. These initial stopping points were found to be unaffected by the calculation conditions. The value of the Cu moment was estimated to be 0.61 μ_B which is within the range of experimental values, proving that our calculation conditions are not so far from the realistic condition.

An important point of our investigation is to estimate the changes in the electronic states around the injected muons as a dilute impurity. We put muon at one of the local minimum potential positions and estimated the changes in the electronic states around that muon.

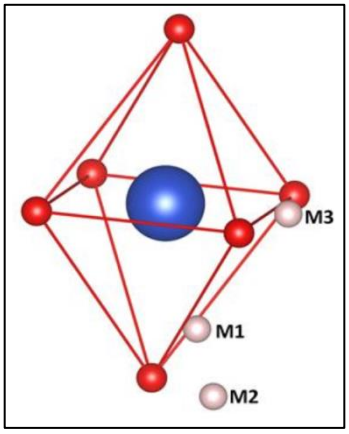

Figure 14. Three minimum positions observed by DFT (muon positions are enlarged for clarity)

Accordingly, we observe the local deformation of the crystal structure caused by M1, M2, and M3 positions. We also found out that the muon stopping position itself will relax self-consistently following the local deformation of the crystal structure caused by the muon. Figure 15 shows these situations, where the muon that stop at the M1 positions moves closer to the Cu atom, while the muons at the M2 and M3 position only affect the nearest planar oxygen positions. We also found that the magnetic moment is affected by the injected muon. This effect was the strongest for the M1 position. Figure 16 (b) shows the change in the magnetic moment of the Cu spin after we place the muon at the M1 position. The magnetic moment shrank around the muon, which confirm the distortion effect by the muon added to the material. As the nearest magnetic moment of the muon was reduced, the expected internal field at the muon site would also change.

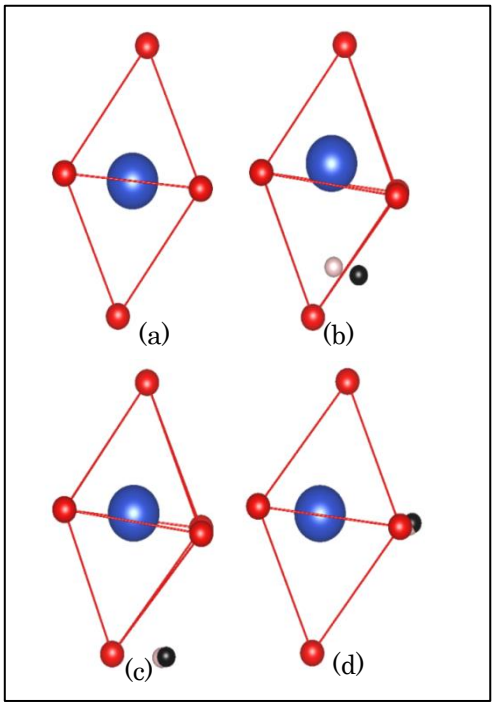

Figure 15: Comparison of CuO_6 octahedral after relaxation (a) Without muon (b) M1 (c) M2 (d) M3. (black sphere shows the positions before relaxation).

By taking into account this effect, we are now estimating the values of the internal field at the muon site and comparing these value with the experimental results.

At this moment, the supercell's size is not sufficient to simulate the muon as a dilute impurity. We are trying to expand the cell size to be 4 x 4 x 2 and 5 x 5 x 3. These calculations will take a longer time and require greater core times even on the BW system. We will proceed this trial in 2018 and try to get the results published.

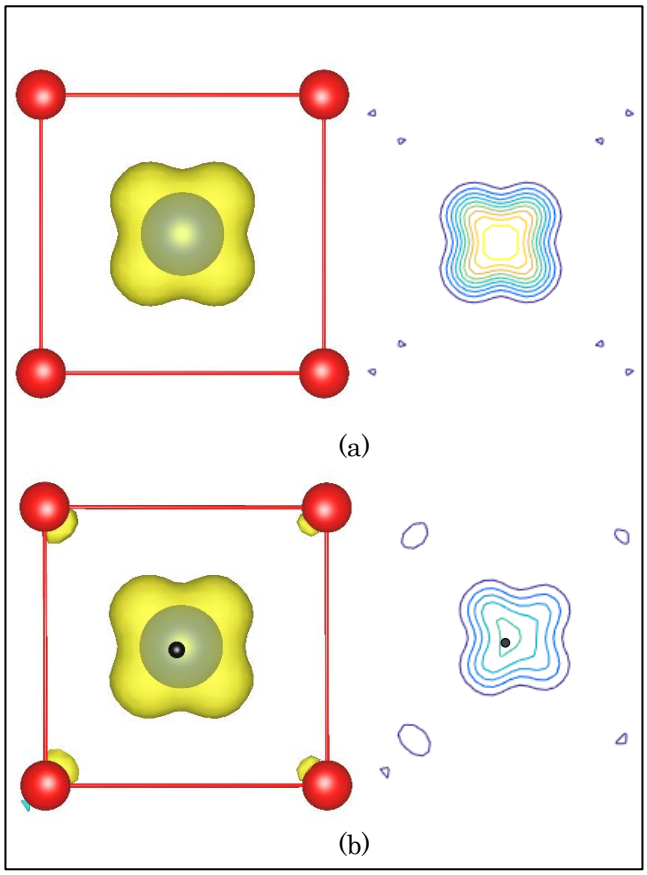

Figure 16: Spin density of CuO_4 plane and its contour at b = 0.5 (a) Without muon (b) M1. (black sphere shows M1 position).

b) $YBa_2Cu_3O_6$ ($YBCO_6$)

The simple dipole-field calculation has failed to explain the μSR data. So, we are trying to estimate muon positions using DFT method, taking into account the quantum effects. In this year, we improved our previous DFT

calculations on $YBCO_6$ and estimated initial muon stopping positions using the larger scale supercell (4×4×2 unit cells) with a finer calculation-grid resolution. Accordingly, we obtained some possible initial muon stopping positions from M1 to M3 as shown in Figure 17. Those muon positions are located at the bottom of the potential energy distribution which causes the quantum distribution of the muon position due to the zero-point vibration motion. We found that the M1 and M2 positions are nearly connected with the zero-point vibrational energy of the muon, indicating that the muon can move around those two positions. We also found that the small component of the magnetic moment appears at the oxygen site which makes the dipole-field calculation condition becomes complicated. We guess that this is due to the strong hybridized state between Cu-3*d* and O-2*p* orbitals.

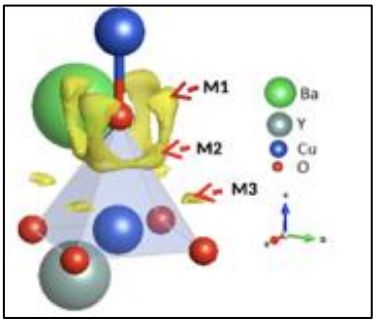

Figure 17: Possible muon sites in $YBCO_6$ as marked M1, M2 and M3. Yellow area indicates an isosurface of minimum potential energy which can be regarded as possible muon stopping positions.

We used hydrogen pseudopotentials to model the muon in the system. We have embedded the muon as a dilute particle in a 4x4x2 supercell, and a full lattice relaxation is taken into account to investigate the local quantum effect caused by the muons. Then, we found that the muon stopped at the M3 position could largely affect the spin state and the local environment surrounding the muon. The magnetic moment of Cu^{2+} changed from about 0.68 μ_B to be smaller with the presence of muon and the small component of the magnetic moment at the nearest oxygen site of the M3 position vanished completely as shown in Figure 18.

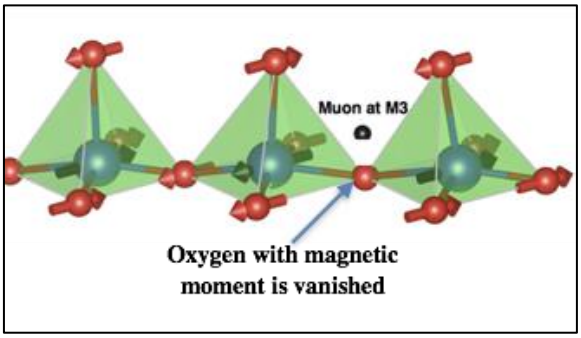

Figure 18: Spin structure of $YBCO_6$ from our DFT calculations.

iii) Synthesized simple and short strand DNA

a) DNA nucleobase and nucleotide

The converged molecular orbitals were used to examine the electronic structures of the systems and the muon hyperfine coupling constant (HFCC) at each possible muon site. The calculation was started with nucleobase and nucleotide structures. The difference between these two structures is that in nucleobase, a methyl group is attached to the base while for nucleotides, a sugar phosphate group is attached to the base (Figure 3).

This study provides insight into the influence of the methyl group and sugar phosphate group to the hyperfine interaction of muon. From the results of our calculations, the presence of methyl group or sugar phosphate group to the nucleic acid bases has a direct effect on the structure of the system which in turn affects the local environment in the vicinity of the muon trapping sites. This is a major factor that influences the electronic structure at the muon trapping site. The results from DFT

calculations also suggest that the most probable muon trapping sites for adenine, guanine, thymine, and cytosine are at the atoms with the unsaturated bonds. The results from our computational studies are tabulated in Tables 1 - 4. Rows that are shaded indicate that the difference in HFCC is large between the nucleobase and nucleotide. Figure 19-22 show the structures of nucleobase and nucleotide for guanine, adenine, cytosine and thymine.

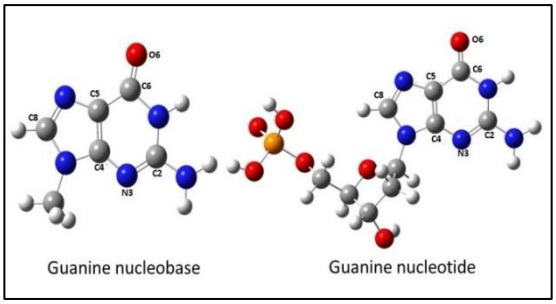

Figure 19: Structure of guanine nucleobase and guanine nucleotide

Table 1: Muonium HFCC at different sites in guanine.

Guanine			
Muonium sites	hfcc (MHz)		% difference
	Nucleobase	Nucleotide	
C6	173.1	74.9	-60
C8	347.9	323.8	-7
O6	0.2	2.5	1150
C5	316	445.2	41
C4	358.7	370.8	3
C2	503.3	253.9	-50
N3	393.2	-7.1	-102

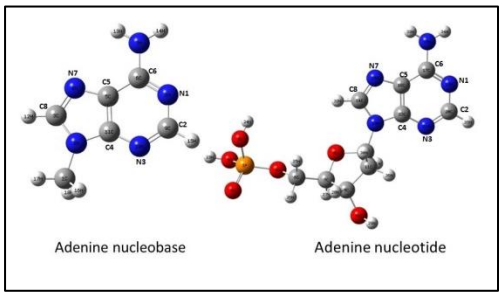

Figure 20: Structure of guanine nucleobase and guanine nucleotide

Table 2: Muonium HFCC at different sites in adenine.

Adenine			
Muonium sites	hfcc (MHz)		% difference
	Nucleobase	Nucleotide	
C8	329	337.1	3
C2	406.6	394.3	-3
N7	47.3	97.8	107
N1	-5.9	-6.4	9
N3	130	179.6	38
C5	475.9	468.1	-2
C4	552.5	535.5	-3
C6	362.5	369	2

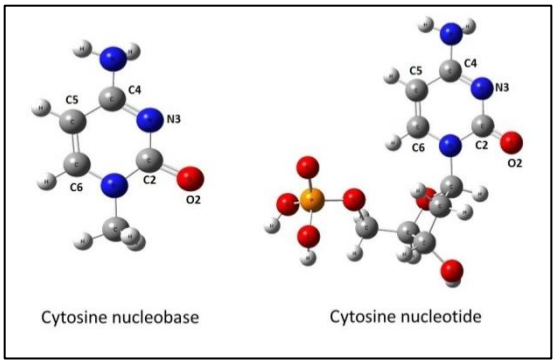

Figure 21: Structure of cytosine nucleobase and cytosine nucleotide

Table 3: Muonium HFCC at differrent sites in cytosine.

Cytosine			
Muonium sites	hfcc (MHz)		% difference
	Nucleobase	Nucleotide	
N3	11.4	5.1	-55
C6	411	428.7	4
C5	377	95.8	-75
O2	3.5	3.7	6
C4	600.8	516.6	-14
C2	1555.3	58.5	-96

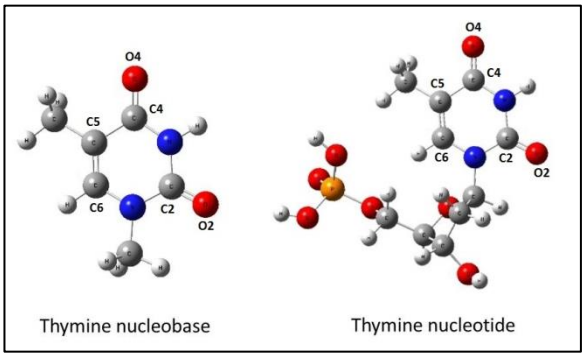

Figure 22: Structure of thymine nucleobase and thymine nucleotide

Table 4: Muonium HFCC at different sites in thymine.

Thymine			
Muonium sites	hfcc (MHz)		% difference
	Nucleobase	Nucleotide	
C6	336.5	339	1
C5	505.3	522.7	4
O4	1.4	360.2	26045
O2	95.6	100.7	5
C4	239.4	8.7	-97
C2	0.7	15.2	1976

b) 12mer Single strand DNA

Currently, the computational work to calculate the HFCC on the 12mer single strand DNA (ssDNA) for adenine, guanine, thymine, and cytosine has been initiated by considering possible muon sites at one of the nucleotides in the middle of the strand. As the number of electrons in the ssDNA is 12 times larger than the single nucleotides it takes a much longer computing time to perform the calculation. The total number of electrons in the 12mer ssDNA oligomers are 1,955, 1,811, 1,907 and 2,051 for A, C, T and G respectively. Therefore, the computational work to investigate muon trapping sites and the associated HFCC at other nucleotides especially the terminal ones is still in progress. The results from this current work have been presented at international conference as listed in the List of Publication section of this report. Most of our all-electron Gaussian16 calculations were performed using ACSL computing resource as our systems consist of large number of electrons.

iv) Kitaev Honeycomb material

The information on the electronic magnetic moments was obtained in the ground state, and the muon stopping site is at the center of the honeycomb network within the range of a 0.5 eV electrostatic potential. The effect of the muon zero-point vibration on the hyperfine interactions was also taken into consideration in our work. In all calculations, on-site Coulomb interactions and Hund's couplings were controlled based on the previous research of a material with the similar crystal environment, Sr_2RuO_4. We compared the free energies of the honeycomb ruthenate for the possible magnetic orders, i.e., zigzag, stripy, Neel typed antiferromagnetic (AF) and ferromagnetic orders. Previous experimental result indicates zigzag antiferromagnetic ordering in the ground state, whereas the results of our calculations show ferromagnetic (FM) ordering in the ground state. The energy of the system in the zigzag AF ordering is found to be slightly higher than when it is in the FM ordered state by about 10 meV which is in the uncertainty range of the density functional theory calculation. After full lattice relaxation of the muonated system, we found that the alignment of the magnetic moments becomes non-collinear, where the alignment on a layer is different from the alignment on other neighboring layers. It was thought that different lattice environments by stacking honeycomb layers lead to non-collinearly aligned magnetic

moments. In order to clarify the relation between the stacking honeycomb layers and the non-collinear alignment, single and double layer cases will be investigated. The calculated dipolar fields at the two muon sites considered in this work are 130 G and 80 G which are not much different from the internal fields of the experimental muon Larmor precessions, approximately 150 G and 60 G. The results will be published after completing this project.

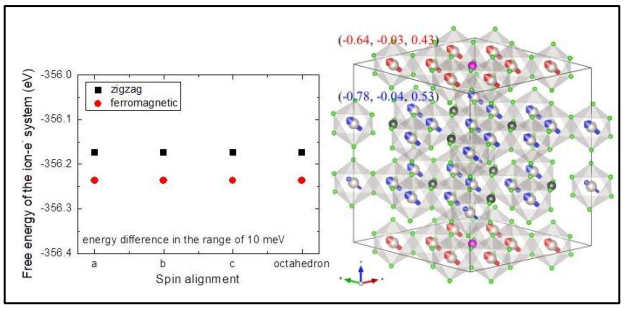

Figure 23: Free energies of the honeycomb ruthenate for the zigzag AF, and ferromagnetic orders (left), and the spin alignment of the honeycomb ruthenate for the ferromagnetic order including muons (right).

v) Gold nano-clusters

First-principle computational studies of the electronic structures (HOMO-LUMO), magnetic structure and spin distribution in these gold nanoparticle systems, particularly for the muonated cases have been performed. At present, our focus is on studying the charge transfer interaction between the core Au and gold thiolate complexes. In the case of the muonated systems, we have started our work with two types of Au_{25} clusters. As shown in Figure 24, there are three distinctive muon sites in Cluster 1; two sites near the gold thiolate complexes and the other one is in the core Au, were examined. In Cluster 2, there is an additional muon site which is at the benzene from the alkyl group that is attached to the thiolate ligand.

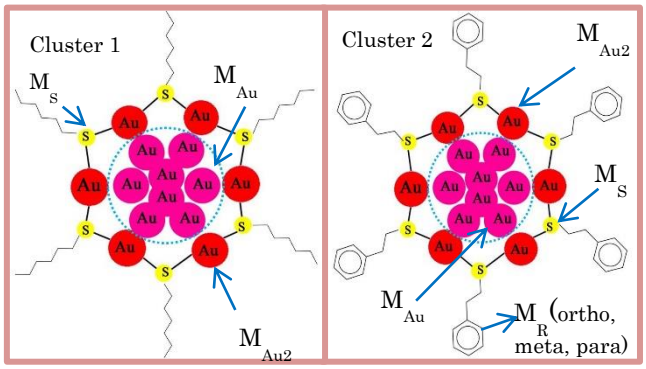

Figure 24: Possible muon sites in $Au_{25}SR_{18}$.(R1= Hexyl, R2= ethyl benzene)

As shown in Table 5, the relative energy results for Cluster 1 show that the most stable muon site is at M_S, which is near the thiolate ligand. The term relative energy refers to the difference of the total energy at a particular muon site with the total energy at M_S. The magnitude of the hyperfine coupling constants (HFCC) for the muon sites are also given in the table.

Table 5: The relative energies of the muonated systems at the three chemically distinct sites for Cluster 1. The relative energy refers to the energy of the system relative to the energy of Site 1.

	Relative Energy (eV)	HFCC (MHz)
M_S	0.00	-0.17
M_{Au}	0.15	-15.19
M_{Au2}	0.19	-8.56

We have also submitted a research grant application to Universiti Sains Malaysia for this particular research interest.

vi) Alkali metal superoxide

a) RbO_2

For the duration of this project we have perform band structure calculation to obtain the insulating states for RbO_2 and CsO_2. In order to achieve this, the value of the on-site Coulomb repulsion, U, was varied until the desired electronic state is obtained. Appropriate value of U is important so that the correct electronic environment is achieved before introducing muon into the system. For the band structure calculation of RbO_2, we have used the same exchange-correlation potential that was used for KO_2, which is the generalized gradient approximation (GGA).

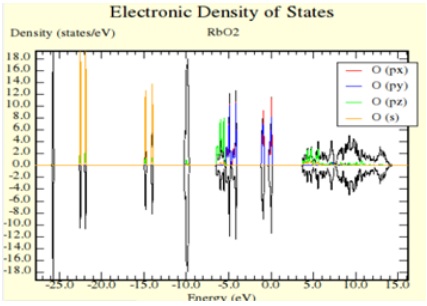

Figure 25 (a): Density of states in RbO_2 using GGA

The insulating state in RbO_2 can be described with the GGA+U. We succeeded to produce the gap at the Fermi level making the system insulating with the optimized U value to be 1.5 eV. Figure 25 (a) and (b) show how the difference in the U value affects the band structure around the Fermi level. In the case of the zero-value at U, the system is nearly insulating but the upper band near the Γ point is very close to the Fermi level, this would made the system slightly metallic at high temperatures. On the other hand, in the case of the U=1.5 eV, the upper band is strongly pushed up above the Fermi level making a large gap against the lower band. These separations of two bands make the system insulating and can be regarded as the Mott system.

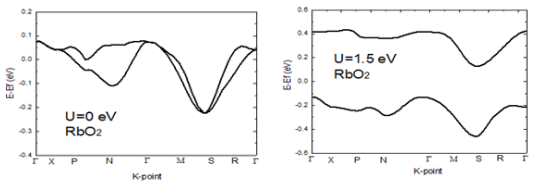

Figure 25 (b): Band structure in RbO_2

b) CsO_2

Several alkali metal superoxides exhibit structural phase transitions. Because of these structural changes, there will be a lowering of the symmetry with a decrease in temperature. The change in the crystal structure causes a splitting of the *p*-orbital degeneracy similar to the Jahn-Teller effect. For the CsO_2, we have calculated the electronic properties for the high symmetry (tetragonal structure) and low symmetry (orthorhombic structure) phases as shown in Figure 26.

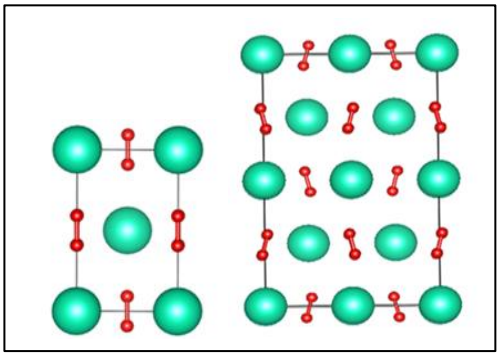

Figure 26: The structure of CsO_2 for the high and low symmetry

To study the electronic properties, we have investigated the band structure and DOS for both phases. We used exchange-correlation potential, the generalized gradient approximation (GGA) for high symmetry and GGA+U on the oxygen *2p* electrons for low symmetry structure. The results are shown below:

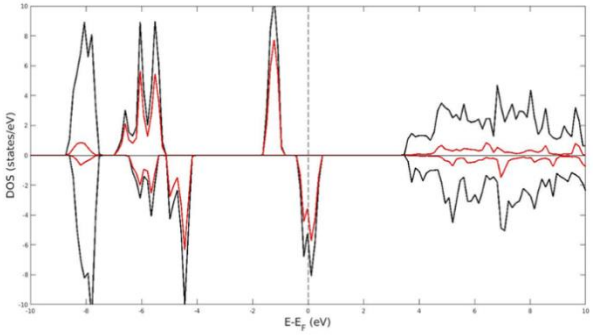

Figure. 27: The DOS using the GGA exchange correlation for the high symmetry phase. The red lines represent the partial DOS of oxygen *2p* and the black line represent the total DOS.

Figure 27 shows the DOS for the CsO_2 in high symmetry phase. There is no splitting mechanism at the Fermi level E_F. This result can also be confirmed from the band structure calculations as shown in Figure 28. The band structure for the low symmetry phase also show that there is no splitting mechanism at the E_F.

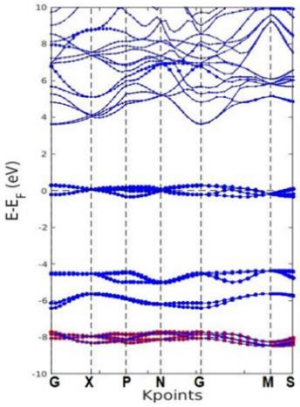

Figure 28: The band structure for the high symmetry CsO_2. The red lines represent the band structure of Cs *2p* and the blue line represent the band structure of oxygen *2p*.

According to Kim *et al.*, 2012, the degenerate π_g states which consists of π_x and π_y states, should be split for an insulation character. Thus, to understand the splitting of the π_g states, we need to consider the effects of the Coulomb correlation of the oxygen *2p* electrons. So, for the low symmetry structure of CsO_2. we applied GGA+U on oxygen. The result is shown in Figures 29 and 30.

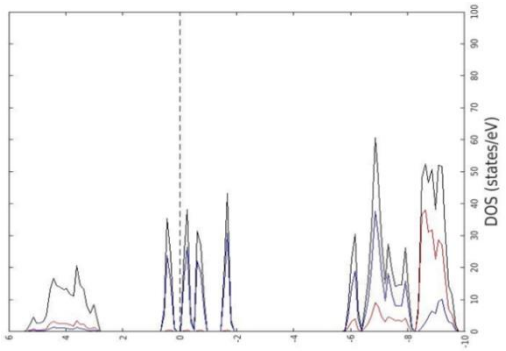

Figure 29: The DOS for CsO_2 at low symmetry

Figure 29 shows the DOS in the GGA+U for the CsO_2 at low symmetry. Note that the U=2 eV. They split only when we applied U=2 eV and above. This result showed the main role of electron correlation effect in CsO_2.

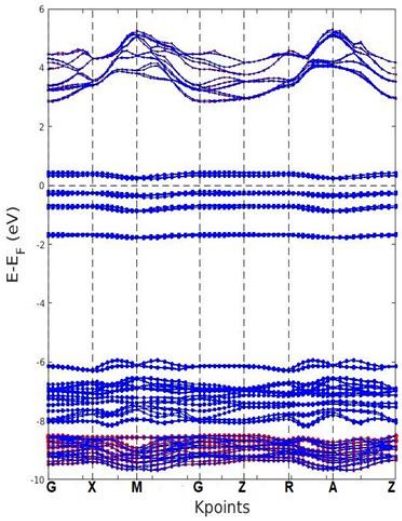

Figure 30: Band structure in CsO_2 at low symmetry

The band structure for CsO_2 showed an insulating state as we applied on site Coulomb repulsion. The gap is open at E_F.

4) Conclusion

Our group has performed DFT calculations on the target systems by using Gaussian16 and VASP. We have succeeded to estimate muon positions in

some organic systems. These results make it possible for us to make comparisons with μSR experimental results. Some of those achievements are now being arranged to be published in scientific journals till the middle of the year of 2018. Among our investigations, especially, the nano-Au cluster is our highlighted system because this system is still in contradiction with regards to its magnetic properties and our computational investigations are the only way to understand this novel electronic property in conjunction with experimental results. In addition to those research achievements, we found in this year that we need strong computing resources to carry out our planned research to simulate large-scale supercells with one muon in order to discuss the muon position and spin states in a realistic situation. We also found that we need more computational power in order to take into account the quantum effects of the muon itself as a fine particle and spatial spin distributions caused by the co-balance bonding among electronic orbitals. These factors are very important for us to proceed with investigations on high-Tc superconductors. We have found that we need about 2 % of the total core time allocated in the BW system in order for us to complete one large-scale calculation on La_2CuO_4 including all quantum effects which must be taken into account. Calculations on high-Tc superconductors are still on-going and we need to perform more optimizations in 2018. Therefore, we require similar computing core times in the GW and BW systems to complete those complicated calculations which can produce high-impact results for this research field and also for the muon community. At this moment, these computational investigations, in conjunction with μSR experiments are in the world-wide competition. We would like to lead this competition by leveraging on RIKEN's high-performance computational resources. We believe that our theoretical results would provide better understandings on the electronic structures of the target materials.

Our accomplishments from these theoretical research have been presented in various international conferences and have also been published, as listed in Form H-2 below. Some of the publications are ready to be submitted.

5) Schedule and prospect for the future

On the basis of our achievements in 2017, we plan to perform more calculations on our target systems and try to gain the following goals. On the other hand, we are going to start to release our achieved experimental and computational results in the year of 2018 because our results are not matured to be published in scientific journals in 2017. Thus, we expect that 2018 will be a productive year. The detailed plans are described in the research plan for 2018, to be submitted to RIKEN after the submission of this report.

i. Organic molecular systems

We put the priority on the investigations on the series of $(BEDT\text{-}TTF)_2X$ system. μSR experimental results have been summarized and already submitted to a journal. Thus, we aim to clarify muon positions on these systems and reveal the magnetic spin structure. These results can be straightforwardly published. We aim to publish our computational results till the summer time. Then, efforts on the series of the $X[Pd(dmit)_2]_2$ system will be followed.

ii. High-Tc superconductors

We will continue to perform large-scale calculations using the supercell model. We still need the optimization of the electronic correlation function and the size of the supercell. We plan to complete those estimations till around the summer of 2018 and we will make comparisons with our experimental results. We will carry out calculations on both La_2CuO_4 and $YBa_2Cu_3O_6$ in parallel, comparing the results of both systems.

iii. DNA

We are getting more μSR experimental results on some synthetic DNA samples to

investigate the electron hopping phenomenon along the DNA chains. Since we have already obtained some computational results as well, we will soon prepare a paper for publication. We expect that we can publish the 1st paper around the summer time. We have more DNA samples and are going to investigate them by experimental and computational methods. Following the 1st publication, we plan to follow the way to publish for those other targets as well.

iv. Kitaev honeycomb systems

We are completing this project and aim to publish as soon as possible. We have obtained sufficient computational and experimental results. We are now discussing how we can release those data as publications in 2018. We plan to publish the 1st paper during the autumn time in 2018. We may carry out some small-size calculations on this system in order to compensate some missing parts.

v. Nano-Au clusters

We are planning to carry out the final μSR experiments within the fiscal year of 2017. Since we have already obtained computational results on those systems, we plan to immediately publish both results after the μSR experiments are completed. This would be expected before the summer.

vi. Alkali metal superoxides

Computational investigations on these systems started in 2017, and we are now still optimizing our calculation parameters. At this moment, we have found a good parameter value for the on-site Coulomb interaction. We will proceed by making more adjustments of the calculation parameters in 2018 and try to simulate the muon position and magnetic spin structures. In addition to this, we plan to try to estimate the transfer integral values between the oxygen dumbbells which are expected to rule out the magnetism of these systems. This parameter is important to discuss the dimensionality of the magnetic interactions.

Since our group's research require powerful and large-scale calculations on each target system, we would like to continue to use both GW and BW systems on HOKUSAI. For the future project, we plan to proceed with the calculations for the transfer integral, Fermi surface, density of state and muon site calculations. Here, we list the next target samples to be studied on the basis of our achievements and experiences. If possible, we would like to start to work on those systems within 2018.

1. λ-$(STF)_2FeCl_4$
2. λ-$(STF)_2GaCl_4$
3. λ-$(BETS)_2FeCl_4$

Fiscal Year 2017 List of Publications Resulting from the Use of the supercomputer

[Proceedings, etc.]

1. Watanabe, I., Yoon, S., Suprayoga, E., Adam, N., Mohd-Tajudin, S. S., Rozlan, A. F., Sari, D. P., Asih, R., Astuti, F., Angel, J., Umar, M. D., Sulaiman, S., & Mohamed-Ibrahim, M. I. (2017).The RIKEN-RAL Muon Facility and the Application of Muons for Studies of Magnetic Properties of Nano-Materials. *Material Science Forum,* 901, 37

[Oral presentation at an international symposium]

1. Sulaiman, S. (February, 2018). DFT Studies on Muon Sites and Associated Hyperfine Interactions in Single Strand DNA. *Oral Presentation at URICAS Symposium 2018.* RIKEN, Japan.

2. Ramli, I., Mohd-Tajudin, S. S., Rozak, H., Sulaiman, S., Mohamed-Ibrahim, M.I., & Watanabe, I. (September, 2017). Muon Sites in High-Tc Superconductor, $YBa_2Cu_3O_6$. *Oral presentation at 3rd Emallia Conference*. Pusan National University, Busan, South Korea.

3. Asih, R., Angel, J., Maeda, S., Sari, D.P., Astuti, F., Matsuhira, K., Wakeshima, K., Hinatsu, Y., Watanabe, I., Nakano, T., & Nozue, Y. (September, 2017). Magnetic Ordered States of Hole Doped Pyrochlore Iridates $(Nd_{1-x}Ca_x)_2Ir_2O_7$ Studied by μSR. *Oral presentation at 3rd Emallia Conference*. Pusan National University, Busan, South Korea.

4. Sari, D. P., & Watanabe, I. (September, 2017). Possible Coexistence of *s-* and *d-* Wave Pairing symmetry in λ-$(BETS)_2GaCl_4$ Studied by µSR. *Oral Presentation at the 3rd Emallia Conference*. Pusan National University, Busan, South Korea.

5. Sulaiman, S. (August, 2017). Computational Investigation of Organic Molecular Systems at Computational Chemistry and Physics Laboratory. *Oral Presentation at RIKEN Symposium: International Workshop on Organic Molecular System*, (pp. 20). Pulau Pinang, Malaysia.

6. Sulaiman, S. (February, 2017). Understanding Electron Transport in DNA: μSR and First Principle Computational Investigations. *Oral Presentation at URICAS Symposium 2017,* (pp.7). INFORMM Universiti Sains Malaysia, Pulau Pinang, Malaysia.

[Others (Press release, Science lecture for the public)]

1. Ramadhan, M. R., Asih, R., Mohamed-Ibrahim, M. I., Sulaiman, S., & Watanabe, I. (October, 2017). Reconsideration of Muon Site in La_2CuO_4 part II. *Poster presentation at JPS meeting*. Moriooka, Japan.

2. Sari, D. P., & Watanabe, I. (September, 2017). Possible Coexistence of *s*- and *d*- Wave Pairing Symmetry in λ-$(BETS)_2GaCl_4$. *Poster presentation at The 12th International Symposium on Crystalline Organic Metals, Superconductors and Magnets 2017*. Miyagi Zao Royal Hotel, Miyagi, Japan.

3. Ramli, I., Mohd-Tajudin, S. S., Rozak, H., Sulaiman, S., Mohamed-Ibrahim, M. I., & Watanabe, I. (September, 2017). Muon Sites in High-Tc Superconductor, $YBa_2Cu_3O_6$. *Poster presentation at Japanese Physical Society Meeting*. Iwate Univeristy, Japan.

4. Rozak, H., Zaharim, W. N., Astuti, F., Asih, R., Zaharim, W. N., Abu Bakar, S. N., Ismail, N., Mohamed-Ibrahim, M. I., Sulaiman, S., & Watanabe, I . (September, 2017). μSR Study on Electron Dynamics in Single Strand Synthetic DNA. *Poster presentation at JPS Autumn Meeting 2017*, (pp. 136). Iwate University, Japan.

5. Umar, M. D., Mohamed-Ibrahim, M. I., Sulaiman, S., and Watanabe, I. (September, 2017). Reconsideration of Muon Sites on La_2CuO_4 Part: I. *Poster presentation at JPS Autumn Meeting 2017*, (pp.121). Iwate University, Japan.

6. Asih, R., Angel, J., Maeda, S., Sari, D.P., Astuti, F., Matsuhira, K., Wakeshima, K., Hinatsu, Y., Watanabe, I., Nakano, T., & Nozue, Y. (August, 2017). Magnetic Ordered States of Hole Doped Pyrochlore Iridates $(Nd_{1-x}Ca_x)_2Ir_2O_7$ Studied by μSR. *Poster presentation at RIKEN Symposium International Workshop on Organic Molecular System*. Pulau Pinang, Malaysia.

7. Ramadhan, M. R., Mohamed-Ibrahim, M. I., Sulaiman, S., & Watanabe, I. (August, 2017). Reconsideration of Muon Site in La_2CuO_4. *Poster presentation at RIKEN Symposium: International Workshop on Organic Molecule Systems*. Pulau Pinang, Malaysia.

8. Ramli, I., Mohd-Tajudin, S. S., Sulaiman, S., Mohamed-Ibrahim, M. I., & Watanabe. (August, 2017). A fast Program for Internal Fields Calculation at the Muon Site. *Poster presentation at International Workshop on Organic Molecular Systems (RIKEN Symposium & Joint Workshop between RIKEN Nishina Center and USM).* Pulau Pinang, Malaysia.

9. Rozak, H., Zaharim, W. N., Astuti, F., Asih, R., Zaharim, W. N., Abu Bakar, S. N., Samsuddin, S., Ismail, N., Mohamed-Ibrahim, M. I., Sulaiman, S., & Watanabe, I. (August, 2017). μSR Studies on Electron Dynamics in Guanine. *Poster presentation at RIKEN Symposium: International Workshop on Organic Molecular System,* (pp. 43). Pulau Pinang, Malaysia.

10. Zaharim, W. N., Rozak, H., Abu Bakar, S. N., Ismail, N., Samian, M. R.,Mohamed-Ibrahim, M. I., Sulaiman, S., & Watanabe, I. (August, 2017). Density Functional Theory Studies on Muon Sites in Deoxyguanlic acid and 9- Methylguanine. *Poster presentation at RIKEN Symposium: International Workshop on Organic Molecular System* (pp. 51). Pulau Pinang, Malaysia.

11. Abu Bakar, S. N., Zaharim, W. N., Rozak, H., Ismail, N., Samian, M. R.,Mohamed-Ibrahim, M. I., Sulaiman, S., & Watanabe, I. (August, 2017). DFT Studies on Muon Stopping Sites in

1-Methylthymine and Thymidine Monophosphate. *Poster presentation at RIKEN Symposium: International Workshop on Organic Molecular System*, (pp. 69). Pulau Pinang, Malaysia.

12. Ismail, N., Zaharim, W. N., Rozak, H., Abu Bakar, S. N., Samian, M. R.,Mohamed-Ibrahim, M. I., Sulaiman, S., & Watanabe, I. (August, 2017). First Principle Study of Muonium Trapping in Deoxycytidine Monophosphate and 1-Methylcytosine. *Poster presentation at RIKEN Symposium: International Workshop on Organic Molecular System* (pp. 55). Pulau Pinang, Malaysia.

13. Mohd-Tajudin, S.S., Nishizaki, T., Kikkawa, A., Adam, N., Suprayoga, E., Watanabe, I., Mohamed-Ibrahim, M. I., & Sulaiman, S. (August, 2017). Muon Site Estimation in $YBa_2Cu_3O_6$. *Poster presentation at RIKEN Symposium: International Workshop on Organic Molecular System* (pp. 37). Pulau Pinang, Malaysia.

14. Ahmad, S. N. A., Sulaiman, S, Mohamed-Ibrahim, M. I., Sabar, S., Mohd-Rosli, N. A., & Watanabe, I. (August, 2017). Density Functional Theory Studies on the Electronic Structures of β'-$X[Pd(dmit)_2]_2$ Organic Magnets in the Antiferromagnetic State. *Poster presentation at RIKEN Symposium: International Workshop on Organic Molecular System*, (pp. 41). Pulau Pinang, Malaysia.

15. Ahmad, S. N. A., Sulaiman, S., Mohamed-Ibrahim, M. I., Yahaya, N. Z., Zakaria, N. S., & Watanabe, I. (August, 2017). Investigating the Electronic Structure and Magnetism of Thiolated Gold Nanoclusters through First-Principle Computational Studies*. Poster presentation at RIKEN Symposium: International Workshop on Organic Molecular System,* (pp. 42). Pulau Pinang, Malaysia.

16. Hasan Baseri, D. F., Sulaiman, S., Mohamed-Ibrahim, M. I., & Watanabe, I. (August, 2017). First Principle Computational Studies on the Electronic Structures of Muonated κ-$(BEDT\text{-}TTF)_2Cu[N(CN)_2]Cl$. *Poster presentation at RIKEN Symposium: International Workshop on Organic Molecular System,* (pp. 45). Pulau Pinang, Malaysia.

17. Rozlan, A. F., Sulaiman, S., Mohamed-Ibrahim, M. I., & Watanabe, I. (August, 2017). Studies on Electronic Structure of Organic Magnet Systems, $EtMe_3Z[Pd(dmit)_2]_2$, (Z=P, As). *Poster presentation at RIKEN Symposium: International Workshop on Organic Molecular System*, (pp. 60). Pulau Pinang, Malaysia.

18. Ramli, I., Mohd-Tajudin, S. S., Asih, R., Angel, J., Sulaiman, S., Mohamed-Ibrahim, M. I., & Watanabe, I. (June, 2017). Muon Sites and Internal Fields in $YBa_2Cu_3O_{6+\delta}$ (δ~0.6). *Poster presentation at International Summer School on HPC Challenges in Computational Sciences*. Boulder, Colorado, USA.

19. Asih, R., Angel, J., Maeda, S., Sari, D. P., Astuti, F., Matsuhira, K., Wakeshima, M., Hinatsu, Y., Watanabe, I., Nakano, T., & Nozue, Y. (March, 2017). Magnetic Ordered States of Hole Doped Pyrochlore Iridates $(Nd_{1-x}Ca_x)_2Ir_2O_7$ Studied by μSR. *Poster presentation at 72th annual meeting of the Physical Society of Japan* (abstract no. 18pK-PS-34). Osaka, Japan.

20. Asih, R., Sari, D. P., Angel, J., Matsuhira, K., Nakano, T., Nozue, Y., & Watanabe, I. (March, 2017). Investigation of Magnetic Ordered States in the Pyrochlore Iridates $(Nd,Ca)_2Ir_2O_7$ Probed by μSR. *RIKEN Accel. Prog.*, Rep. 50, 23.

21. Sari, D. P., Asih, R., Hiraki, K., Ishii, Y., Nakano, T., Nozue, Y., & Watanabe,I. (March, 2017). Study of muon spin rotation of the superconductor λ-$(BETS)_2GaCl_4$. *RIKEN Accel. Prog*. Rep. 50, 240.

22. Rozak, H., Zaharim, W. N., Astuti, F., Asih, R., Zaharim, W. N., Abu Bakar, S. N., Ismail, N., Mohamed-Ibrahim, M. I., Sulaiman, S., and Watanabe, I. (February, 2017). *μSR* Studies on Electron Dynamics in Guanine. *Poster presentation at URICAS Symposium 2017*, (pp.12). INFORMM, Universiti Sains Malaysia, Pulau Pinang, Malaysia.

23. Zaharim, W. N., Rozak, H., Abu Bakar, S. N., Ismail, N., Samian, M. R.,Mohamed-Ibrahim, M. I., Sulaiman, S., and Watanabe, I. (February, 2017). Density Functional Theory Studies on Muon Sites in DNA. *Poster presentation at URICAS Symposium 2017*, (pp.25). INFORMM, Universiti Sains Malaysia, Pulau Pinang, Malaysia.